



CHALMERS
UNIVERSITY OF TECHNOLOGY

Propagating Surface Plasmon Polaritons: Towards Applications for Remote-Excitation Surface Catalytic Reactions

Downloaded from: <https://research.chalmers.se>, 2024-04-19 16:14 UTC

Citation for the original published paper (version of record):

Zhang, Z., Fang, Y., Wang, W. et al (2016). Propagating Surface Plasmon Polaritons: Towards Applications for Remote-Excitation Surface Catalytic Reactions. *Advanced Science*, 3(1). <http://dx.doi.org/10.1002/advs.201500215>

N.B. When citing this work, cite the original published paper.

Propagating Surface Plasmon Polaritons: Towards Applications for Remote-Excitation Surface Catalytic Reactions

Zhenglong Zhang, Yurui Fang, Wenhui Wang, Li Chen, and Mengtao Sun*

Plasmonics is a well-established field, exploiting the interaction of light and metals at the nanoscale; with the help of surface plasmon polaritons, remote-excitation can also be observed by using silver or gold plasmonic waveguides. Recently, plasmonic catalysis was established as a new exciting platform for heterogeneous catalytic reactions. Recent reports present remote-excitation surface catalytic reactions as a route to enhance the rate of chemical reactions, and offer a pathway to control surface catalytic reactions. In this review, we focus on recent advanced reports on silver plasmonic waveguide for remote-excitation surface catalytic reactions. First, the synthesis methods and characterization techniques of silver nanowire plasmonic waveguides are summarized, and the properties and physical mechanisms of plasmonic waveguides are presented in detail. Then, the applications of plasmonic waveguides including remote excitation fluorescence and SERS are introduced, and we focus on the field of remote-excitation surface catalytic reactions. Finally, forecasts are made for possible future applications for the remote-excitation surface catalysis by plasmonic waveguides in living cells.

1. Introduction

Surface plasmons (SPs) are the collective oscillations of free electrons that are confined evanescently on a metal surface.^[1] Coupled with photons, SPs can act as a collective excitation of conduction electrons that propagate in a wave like manner along an interface between a metal and a dielectric, known as surface plasmon polaritons (SPPs). SPPs are confined to the vicinity of the interface and can propagate along the metal surface until the energy dissipates, either by heat loss or by radiation into free space.^[2] Localized surface plasmons (LSPs) are oscillations of charge density that are confined on the metallic nanoparticle's surface. The resonant LSPs, known as LSPR, result in a large enhancement of the localized electromagnetic (EM) field, which is the underlying mechanism for surface enhanced spectroscopy.

LSPs and SPPs have been widely used in plasmonic resonance sensors,^[2,3] tip-/surface-enhanced Raman spectroscopy, so-called TERS/ SERS,^[4,5] and plasmonic catalysis,^[6] etc.

Since their discovery, SERS and TERS have extensively been experimentally and theoretically studied because of their extremely high sensitivity and wide applications in qualitative and quantitative analysis by fingerprint vibrational spectroscopy, even at the single-molecular level.^[7–14] In addition, due to the high throughput and low energy requirements, a novel application of plasmonics in chemical reactions gains significant attention, as reported in works on dissociation of hydrogen^[15,16] and water,^[17,18] photochemical^[19–23] and plasmon-driven chemical reactions,^[24–37] etc. SPs excited on the surface of gold or silver can non-radiatively decay into so-called hot electrons with a high energy between the Fermi and vacuum energy level.^[36–40] The hot electrons could scatter into the absorbed molecule's excited state and then trigger chemical reactions by reducing the activation energy, so-called plasmonic catalysis.^[41] If the reaction is monitored by SERS or TERS spectra, the nanostructures behave as catalysts and nanoscale signal enhancers, simultaneously. Plasmon catalyzed reactions monitored by TERS and SERS have been reviewed by many different groups.^[5,6,42–47]

Currently, the plasmonic waveguide has been successfully applied in the field of remote-excitation surface enhanced Raman spectroscopy.^[48,49] Compared with traditional SERS, remote excitation SERS has many advantages. In normal

Dr. Z. L. Zhang, Dr. Y. R. Fang, Prof. W. H. Wang,
Dr. L. Chen, Prof. M. T. Sun
Beijing National Laboratory for
Condensed Matter Physics
Institute of Physics
Chinese Academy of Sciences
Beijing 100190, P.R. China
E-mail: mtsun@iphy.ac.cn

Dr. Z. L. Zhang
Leibniz Institute of Photonic Technology
Albert-Einstein-Str. 9, 07745 Jena, Germany

Dr. Y. R. Fang
Division of Bionanophotonics
Department of Applied Physics
Chalmers University of Technology
Gothenburg SE-412 96, Sweden

Prof. W. H. Wang
School of Science
Xi'an Jiaotong University
Xi'an 710049, China

Dr. L. Chen
Material Science and Engineering
University of California
San Diego, CA 92093, USA

This is an open access article under the terms of the Creative Commons Attribution License, which permits use, distribution and reproduction in any medium, provided the original work is properly cited.

DOI: 10.1002/advs.201500215



SERS, the excited light is focused on the detected spot, which is called local SERS. In contrast in the 'remote SERS', the excited spot is far away from the detected target, which is excited by the SPPs with a 'remote mode'. Ag or Au waveguides offer a way to go below the size limit because they transfer optical signals via SPPs. SPPs can propagate along the metal waveguide and emit free photons at imperfections or at the end of waveguide, while some of them are lost due to the Ohmic damping. The energy transfer from the spot of illumination and the hot-spot can be mainly supported by the remote systems based on plasmonic waveguide, as illustrated in **Figure 1**. The SPPs could of course excite the nanoscale hot-spot remotely, which can avoid the strong background noise because of a large area of the excited spot, and isolate heat effects from the area of excited light to the target excited in the area of sub-diffraction wavelength. Moreover, it can reduce the possibility of the sample damage by high laser excitation. Based on surface-enhanced spectroscopy, a novel way of sensing measurements can be provided by such a remote SERS system, and it can be used in systems where normal SERS is unsuitable, such as Raman and fluorescence detection of biomolecules in living cells.^[50–52]

It is important that the plasmon-catalyzed reactions can be remotely driven by silver plasmonic waveguides.^[53–55] In the plasmon-driven chemical reactions via the traditional SERS method, the laser is directly radiated on the molecules and metal substrate. Several environmental factors for the plasmon-driven chemical reactions are difficult to clearly exclude, such as photons generated directly from light of the laser, electrons directly escaping from the metal surface by overcoming the work function (photoelectric effect), and heating effect of the laser or surface plasmonic resonance. The plasmonic-waveguide-driven surface catalytic reactions can provide more confident evidence for the mechanism and nature, since the above several environment factors can be explicitly excluded.

In this review, we introduce the recent progress of the propagating SPP (plasmonic waveguide) driven surface catalytic reaction. First, we introduce the synthesis and characterization of plasmonic waveguides of Ag nanowires (NW), and the propagating mechanism of the Ag nanowire is physically revealed. Then, we focus on the application of plasmonic waveguide for remote-excitation research, including fluorescence and SERS, and surface catalyzed reaction of *pp'*-dimercaptoazobenzene (DMAB), as revealed by remote excitation SERS spectroscopy. DMAB can be produced from *para*-aminothiophenol (PATP) and 4-nitrobenzenethiol (4NBT) by propagating SPPs; plasmonic waveguide-driven reduced and oxidized reactions, respectively. Finally, we provide an outlook for possible future applications on remote-excitation surface catalytic reactions in living cells.

2. Synthesis of Ag Nanowire Waveguides

Detection of plasmonic waveguide for remote-excitation surface catalytic reactions requires smooth surfaces, controllable size, and high crystallinity, as these factors decrease dissipative energy loss. SPPs in the visible spectrum can propagate with the least energy loss over tens of micrometers on silver nanowire. Lots of methods have been reported on the synthesis



Zhenglong Zhang is a post-doctoral and AvH fellow at the Leibniz Institute of Photonic Technology, Jena, Germany. He obtained his Ph.D. in 2013 from Shaanxi Normal University and the Institute of Physics, Chinese Academy of Sciences, China, working on STM-based HV-TERS. His current research interests focus on TERS and Plasmonic catalysis.



Yurui Fang obtained his Ph.D. degree from the Institute of Physics, Chinese Academy of Sciences, China in 2011. From 2011 to the present, he has been a postdoctoral researcher in the Department of Applied Physics, Chalmers University of Technology, Sweden. His current research is mainly focused on plasmonic chirality, plasmonic

sensing, hot electron assisted solar cell and sensing, HV-TERS, SERS, plasmonic waveguide and plasmon-driven chemical reactions of organic molecules.



Mengtao Sun is an Associate Professor at the Institute of Physics, Chinese Academy of Sciences, (CAS), China, since 2006. He obtained his Ph.D. in 2003 from the State Key Laboratory of Molecular Reaction Dynamics, Dalian Institute of Chemical Physics, CAS. From 2003 to 2006, he worked as a postdoctoral researcher at the Department

of Chemical Physics, Lund University, Sweden working on photoinduced charge transfer in organic solar cells. His current research interests focus on HV-TERS, SERS, and plasmon-driven chemical reactions.

of silver nanowires such as solution-phase, vapor-phase,^[56,57] and microfabrication techniques.^[58] Ag NWs prepared by lithography methods, however, have the disadvantages of producing polycrystalline structures that have inevitable defects due to the metal evaporation process. These disadvantages can significantly shorten the propagation distance of SPP in NW waveguides by increasing scattering loss.^[58] On the other hand, controlling the diameter and morphology of Ag NWs through the vapor-phase method is difficult.

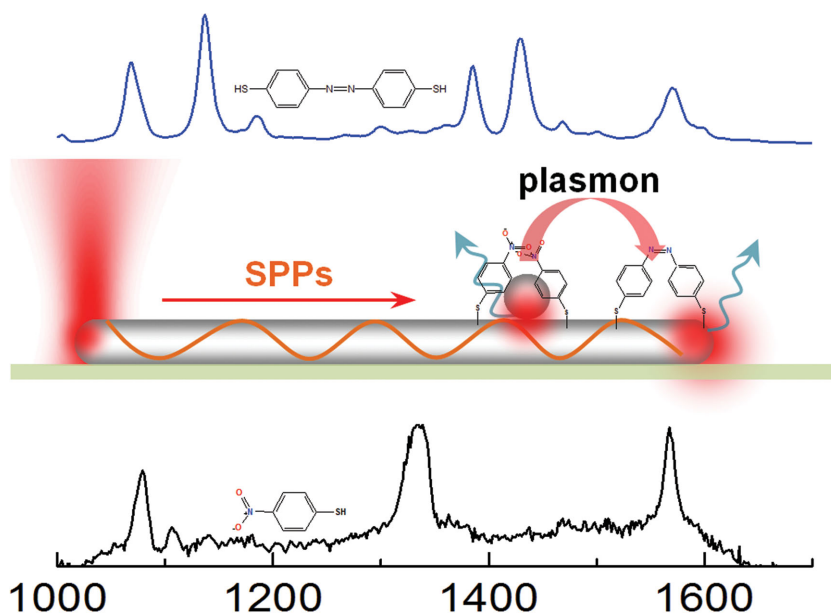


Figure 1. Sketch of remote SERS based on a silver nanoparticle–nanowire system. Raman signals obtained from the excited side is local SERS, while the signals collected at the junction where energy comes from propagating SPPs is remote SERS.

Solution-phase methods are divided into template and non-template methods.^[59,60] The advantage of the template method is that it produces NWs with the desired morphology and high aspect ratio. Various one-dimensional structures such as carbon nanotubes,^[61] mesoporous silica,^[62] alumina or polymer membranes,^[63–66] DNA chains,^[67] and rodlike micelles^[67] are used as templates. However, it is too complex, and the shape and structure of the synthesized NWs are strongly dependent on the use of corrosive chemicals during template dissolution. These disadvantages may be avoided by adopting nontemplate solution-phase methods.^[68] Nontemplate methods include the solution-phase polyol process, which was developed by Xia et al.^[69,70] It is widely used to prepare Ag nanowires with uniform morphology and size (Figure 2).^[71] Silver nitrate in this process is reduced by ethylene glycol with vinyl pyrrolidone (PVP). Here, ethylene glycol is used not only as a solvent but also as a reducing agent, and PVP is used as a surfactant.^[69] The obtained silver atoms deposit onto seeds and grow into NWs with the aid of PVP. The reaction occurs at 160 °C. Agents such as NaCl, CuCl₂, FeCl₃, and PtCl₂ may be added to the solution to ensure nanowire formation.^[70,72–74] In this approach, the size of NWs is well-controlled to within tens to hundreds of nanometers; their length can reach 100 μm. The morphology and size of NWs can be very precisely controlled by manipulation of experimental parameters

such as reaction time, temperature, chemical ratio, injection speed, stirring speed, and added agents.^[75–82] Furthermore, the structure of synthesized Ag NWs is highly crystalline, and the surfaces are very smooth. Dissipative energy loss can be drastically suppressed, and NWs can thereby be efficiently used in plasmonic waveguides for remote-excitation surface catalytic reactions (Figure 3).

3. Characterization of SPPs Propagating on Ag NW Waveguides

3.1. Basic Modes of SPP in Metal Cylindrical NW

This review is mainly concerned with SPP propagation in Ag NW waveguide, and most of the previous works consider a cylindrical shape of NW. Herein, we first describe SPP modes in an infinite cylinder. For an infinite cylindrical wire with radius R and permittivity ϵ_2 in a homogeneous medium (ϵ_1 , a nonmagnetic material), Chang et al. describe the electric and magnetic field as follows:^[83]

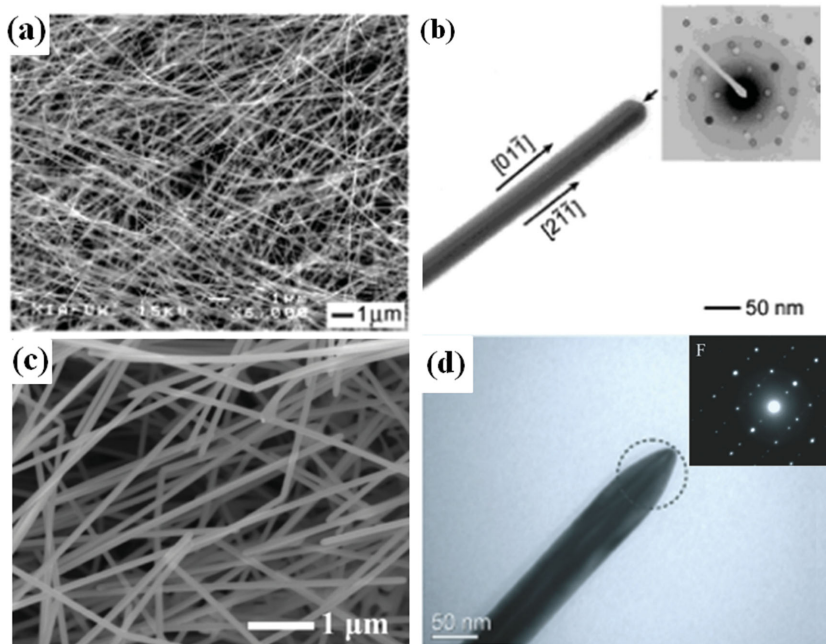


Figure 2. Chemical synthesized Ag NWs. a) SEM images of Ag NWs prepared through the conventional polyol synthesis process. b) TEM image of a Ag NW, demonstrating the bicrystallinity and corresponding growth directions. The inset shows the micro-diffraction pattern recorded by focusing the electron beam onto this NW. c) SEM image of Ag NWs obtained via ammonium carbonate-mediated polyol synthesis method. d) TEM image of an individual NW and the inset shows the selected-area electron diffraction (SAED) patterns taken from the part indicated by the dotted circles. a,b) Reproduced with permission.^[70] Copyright 2002, American Chemical Society. c) Reproduced with permission.^[71] Copyright 2002, American Association for the Advancement of Science. d) Reproduced with permission.^[82] Copyright 2014, Elsevier.

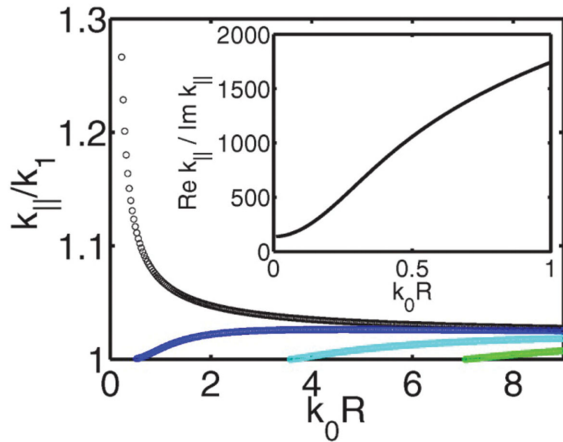


Figure 3. Allowed surface plasmon modes as a function of Ag NW radius (R). The surrounding dielectric $\epsilon_1 = 2$ corresponding wavelength $\lambda_0 = 1 \mu\text{m}$. The $m = 0, 1, 2, 3$ are shown in black, blue, light blue, green. Reproduced with permission.^[83] Copyright 2007, American Physical Society.

$$\mathbf{E}_j(\mathbf{r}, t) = \left\{ \begin{aligned} & \left[\frac{im}{k_j \rho} a_j F_{j,m}(k_{j\perp} \rho) + \frac{ik_{||} k_{j\perp}}{k_j^2} b_j F'_{j,m}(k_{j\perp} \rho) \right] \\ & + \left[-\frac{k_{j\perp}}{k_j} a_j F'_{j,m}(k_{j\perp} \rho) - \frac{mk_{||}}{k_j^2 \rho} b_j F_{j,m}(k_{j\perp} \rho) \right] \hat{\phi} \\ & + \frac{k_{j\perp}^2}{k_j^2} b_j F_{j,m}(k_{j\perp} \rho) \hat{z} \end{aligned} \right\} e^{i(m\phi + k_{||}z - \omega t)} \quad (1)$$

$$\mathbf{H}_j(\mathbf{r}, t) = -\frac{i}{\omega \mu_0} k_j \left\{ \begin{aligned} & \left[\frac{ik_{||} k_{j\perp}}{k_j^2} a_j F'_{j,m}(k_{j\perp} \rho) + \frac{im}{k_j \rho} b_j F_{j,m}(k_{j\perp} \rho) \right] \hat{\rho} \\ & + \left[-\frac{mk_{||}}{k_j^2 \rho} a_j F_{j,m}(k_{j\perp} \rho) - \frac{k_{j\perp}}{k_j} b_j F'_{j,m}(k_{j\perp} \rho) \right] \hat{\phi} \\ & + \frac{k_{j\perp}^2}{k_j^2} a_j F_{j,m}(k_{j\perp} \rho) \hat{z} \end{aligned} \right\} e^{i(m\phi + k_{||}z - \omega t)} \quad (2)$$

where $j = 1, 2$, a condition that pertains to the medium and wire. $F_{1,m}(x) = H_m(x)$ and $F_{2,m}(x) = J_m(x)$ are the Hankel and Bessel functions, respectively. $k_j^2 = k_{j\perp}^2 + k_{j||}^2$ and $k_{j\perp}^2 = \frac{\omega}{c} \sqrt{\epsilon_j}$. a_j, b_j are coefficients that are determined by boundary conditions. From the boundary condition, four equations can be obtained under the following condition:

$$M(a_1 a_2 b_1 b_2)^T = 0 \quad (3)$$

A solution only exists when

$$\det M = 0 \quad (4)$$

According to the results of Chang et al., only lower-order modes ($m = 0, \pm 1$) could exist for thin metal wires; such modes are commonly used (Figure 3), and higher modes are thus excluded. The mode having which $m = 0$ always exists; the thinner the wire is, the more confined the electromagnetic field. For the mode in which $m = \pm 1$, there is no strict cutoff radius, but for a very small radius, the mode volume is very large. For the normal wires we used, modes for which $m = 0$ and $m = \pm 1$ exist. For very thick wires

($R > 150 \text{ nm}$ in air), higher modes exist. For the cases discussed in this paper, only normal wires ($R \approx 100 \text{ nm}$) are considered.

3.2. SPP modes of Ag NW by One End Excitation

In order to excite SPP in the NW, the simplest and most convenient way is directly focusing the light on one end of wire, due to the fact that local symmetry-breaking at a finite length NW terminus is sufficient to excite SPP. Assuming that the harmonic monochromatic laser beam with electric field $\mathbf{E}_{\text{inc}}(\mathbf{r}) = \mathbf{E}_0(\mathbf{r}) \cdot e^{-i\omega t}$ illuminate on the end of wire perpendicular to the wire, the modes on the wire will be excited with the following form (ignoring the time factor):

$$\mathbf{E}^j(\mathbf{r}) = \sum_m \hat{A}_m^j F_m^j(k_{m\perp}^j \rho) \cos m\phi \cdot e^{ik_{m||}z} \quad (5)$$

$m = 0, \pm 1$ corresponding to the modes which can be excited. For an ideal cylinder, in the electrostatic approximation, when the polarization is along the wire, $m = 0$ mode will be excited as

$$\mathbf{E}^j(\mathbf{r}) = \hat{A}_0^j F_0^j(k_{0\perp}^j \rho) e^{ik_{0||}z} \quad (6)$$

If the polarization perpendicular to the wire, $m = \pm 1$ modes will be excited. According to the boundary condition, these are

$$\mathbf{E}_1^j(\mathbf{r}) = \hat{A}_1^j F_1^j(k_{1\perp}^j \rho) \cos m\phi \cdot e^{ik_{1||}z} \quad (7)$$

Where $j = 1, 2$ refer to the medium around and wire. $F_m^1(x) = H_m(x)$, $F_m^2(x) = J_m(x)$ are the Hankel and Bessel functions, respectively. $\hat{A}_m^j = a_m^j \hat{\rho} + b_m^j \hat{\phi} + c_m^j \hat{z}$ is the vector coefficient.

As Figure 4 shows, the wire excited by a paraxial Gaussian beam with an instantaneous electric field of the form $E_{\text{inc}} = E_0 e^{-i\theta}$, where θ is the phase of incident light.^[84] The fundamental $m = 0$ SPP mode or $m = -1$ is selectively excited

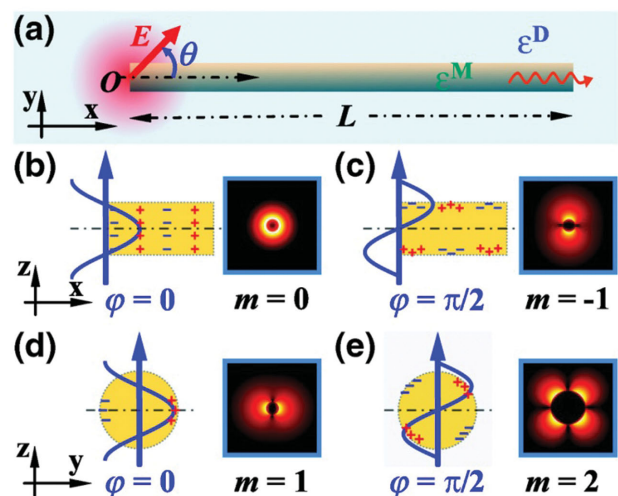


Figure 4. a) Schematic of excitation of plasmon modes in metallic NW in homogeneous environment. b–e) Plasmon modes excited at different incident polarization angle θ and incident phase ϕ . Reproduced with permission.^[84] Copyright 2011, American Physical Society.

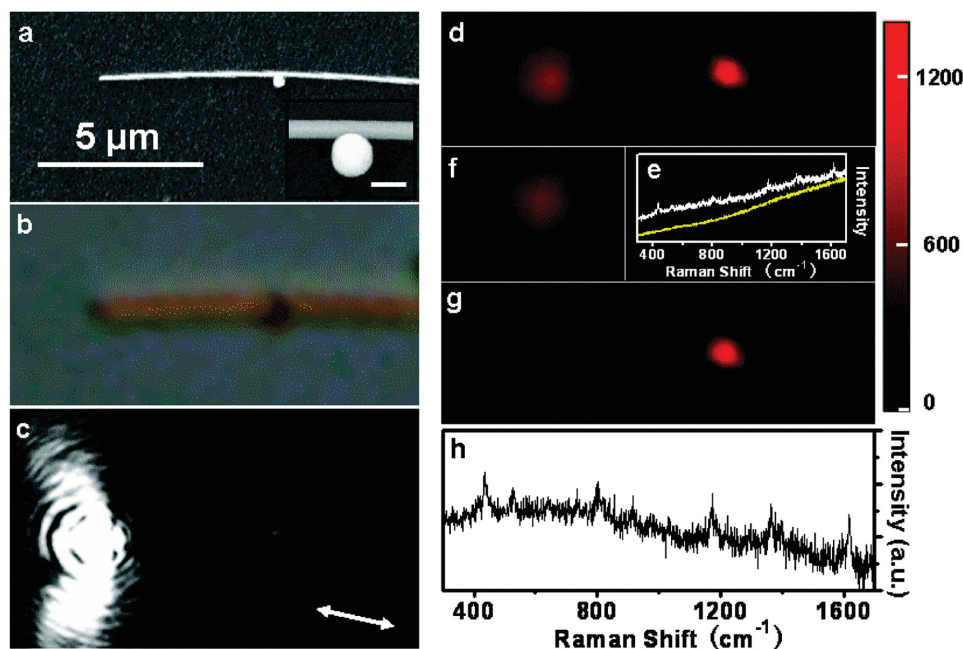


Figure 5. Remote-excitation SERS of MGITC molecules excited through propagating plasmons. a) SEM, b) optical and c) SPP images of a nanowire–nanoparticle system. The corresponding Raman d) image and e) spectra of the Raman peak at 436 cm^{-1} excited at the left end of the nanowire. f) The fluorescence background image of smooth ITO glass only. g) The Raman image after background subtraction of panel (d) from panel (f). h) The remote-excitation SERS spectrum after fluorescence background correction with the spectra taken from panel (e). Reproduced with permission.^[49] Copyright 2009, American Chemical Society.

when the input light phase is $\varphi = 0$ or $\varphi = \pi/2$ with the polarization component along the wire. The $m = 1$ mode is generated for $\varphi = 0$ with polarization components perpendicular to the wire. For any polarization, the light can be divided into the two basic components with polarization along or perpendicular to the wire. The amplitude of the components excited is strongly depending on the polarization angle and of course, the shape of the illuminating terminal.

4. Plasmonic Waveguide for Remote-Excitation

4.1. Features of Remote-Excitation SERS and Early Applications

SPPs propagating on noble-metal nanowires have been widely studied in this decade, which sought to find the basic physical

mechanism.^[58,83–87] In 2009, remote SERS on single silver nanowire systems was investigated by Fang et al.^[49] Remote excited SERS of MGITC molecules was reported, alongside the polarization dependence on the single Ag nanowire with a nanoparticle that was excited by 632.8 nm wavelength (Figure 5). The corresponding SEM, optical and SPP images are shown in Figure 5a–c. Normal SERS spectra of MGITC were obtained from the excited laser spot at left-end of the Ag nanowire or the remote site of the gap of nanowire and nanoparticle, respectively. The remote SERS spectra were obtained from the remote site by separating the signal collection spot from the laser spot. Clearly, the remote excitation SERS spectra can be observed by a single Ag nanowire waveguide after the correction of fluorescence background. It was explained by a two-step mechanism in the numerical simulation. First, the SPs are excited and propagate to the target spot; there is an electromagnetic field

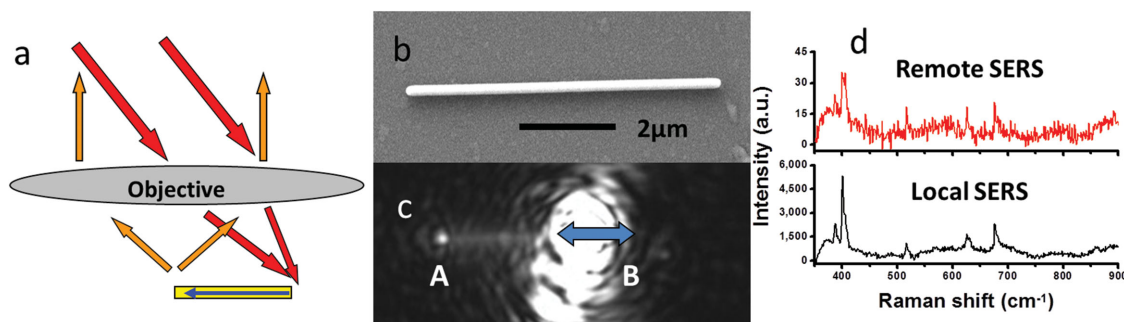


Figure 6. a) Sketch of remote SERS based on a single gold nanowire. b) SEM image and c) the corresponding SPPs image of the gold nanowire waveguide. d) The top remote SERS spectrum (red line) collected at terminus A and the bottom local SERS spectrum (black line) obtained at terminus B. Reproduced with permission.^[87] Copyright 2011, American Chemical Society.

intensity enhancement (F_1) for the excited wavelength. Then the intensity enhancement (F_2) for the local structure of the target spot is achieved for the specific Raman peak wavelength. The product of the two factors gives the remote-excitation SP signal enhancement. This mechanism works for the other systems in this review, while for the remote-excitation catalysis, the first factor (for the laser) dominates, as the hot electrons are excited by the laser excited SPPs; the second factor mainly contributes to the Raman measurement of the catalyzed products. The Raman signal is also remotely detectable as part of the energy is converted to SPPs again as well.

Remote SERS was also measured by a single Au nanowire (Figure 6).^[87] It was found that the remote excitation SERS is dependent on the polarization of the laser. Maximal Raman signals were obtained when the incident polarization is parallel to the nanowire waveguide. In this remote system based on a single nanowire waveguide, the polarization of the remote site could be set toward a specific direction by adjusting the polarization of the excited laser. This procedure, however, requires a previous measurement. Because of their antioxidant property, working time for the operation of Au plasmonic devices may be much longer under ambient environments compared with that of Ag plasmonic devices.

The plasmonic waveguide for remote excitation has been tentatively used in the field of biology, chemistry and physics. In 2012, Yang's group reported a remote system based on nanowire for endoscopy in a cell, *in vivo*.^[50] The remote endoscopy consists of single nanowire of SnO₂ attached to an optical fiber (Figure 7) by using a three-axis micro manipulating system. The inserted SnO₂ nanowire could work as an optical waveguide supporter at the designated positions *in vivo* cells. The sub-cellular images and the fluorescence of the quantum dots emitted at 655 nm in single cell were presented by using nanowire endoscope. In sub-cellular spectra detection in remote endoscope system, the SnO₂ nanowire was located around the preloaded quantum dots, which can be excited by 442 nm wavelength laser. As shown in Figure 7e, the fluorescence signals of quantum dots in cell could be then collected by the remote nanowire waveguide connected with a spectrometer and CCD. To achieve a larger intensity of the remote signals, a Ag or Au nanowire waveguide can be used to replace the semiconductor nanowire because of the enhanced electromagnetic of SPPs.

In 2014, Uji-i et al. reported the remote excitation SERS by plasmonic waveguide in living cell.^[51] As shown in Figure 8, the plas-

monic hotspot (at the gap of two Ag nanowires, or at the gap of nanowire and nanoparticles) on the Ag nanowire probe inserted into the cells was excited by SPPs, and the signals were collected from the other side the Ag nanowire probe outside the cells. A clear remote SERS spectrum can be observed by using an Ag nanowire probe hotspot inserted into a living HeLa cell.

Clearly, it is possible that plasmonic waveguide of a single metal nanowire can be used for remote excitation in living cell system. In addition, this remote excitation technique can also be used for another important application known as plasmon driven chemical reactions.

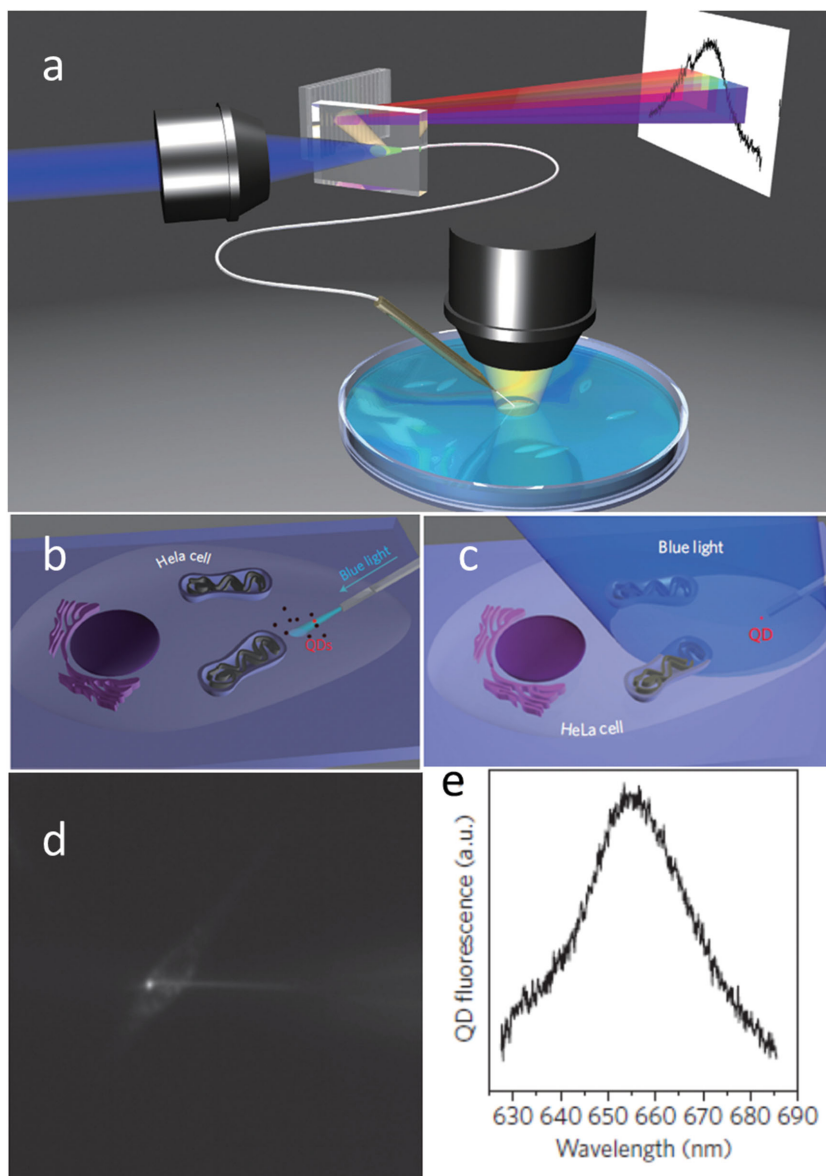


Figure 7. a) A sketch of the remote nanowire endoscope system *in vivo* cells. b) A sketch of sub-cellular imaging and c) local spectrum remotely collected in a cell *in vivo* through the system. d) The dark field image of the remote detection of quantum dot fluorescence in a cell *in vivo*. e) The corresponding spectrum remotely collected through the nanowire endoscope system. Reproduced with permission.^[50] Copyright 2012, Nature Publishing Group.^[50]

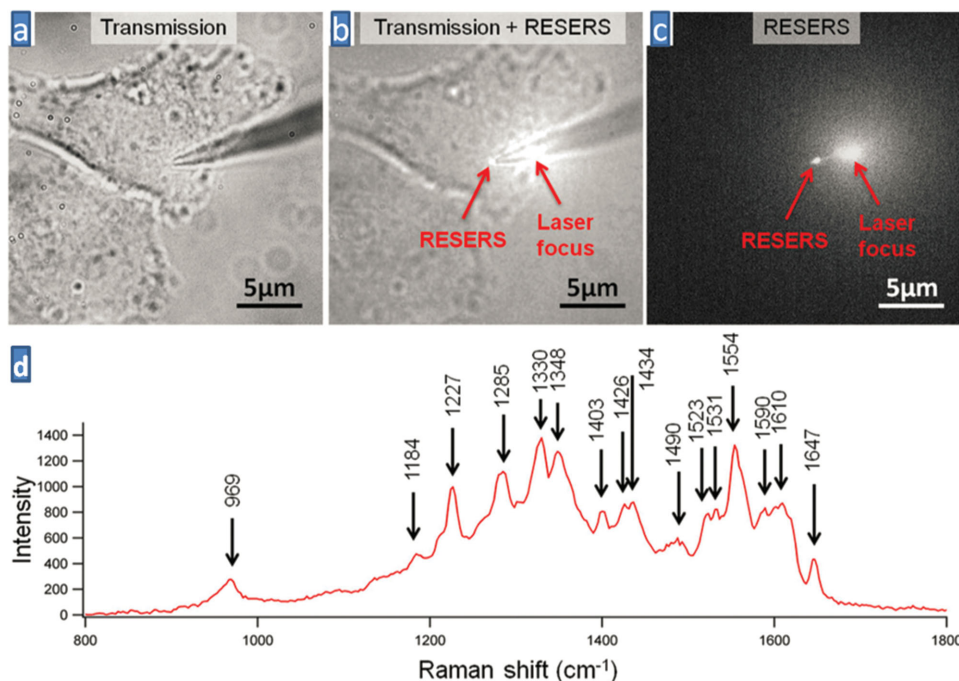


Figure 8. Scheme of the positions chosen for remote-excitation SERS spectroscopy inside a live HeLa cell during Ag NW probe endoscopy. a–c), Remote excitation SERS endoscopy of a live HeLa cell. a) Optical transmission, b) combination of optical transmission and remote excitation SERS, and c) remote excitation SERS only images of a Ag NW probe in a live HeLa cell. d) A remote excitation SERS spectrum from the nucleus of the live HeLa cell. Reproduced with permission.^[51]

4.2. Remote-Excitation Plasmon-Driven Chemical Reaction

4.2.1. Features of the Plasmon-Driven Chemical Reaction

Assisted by the plasmon-induced hot electrons, plasmonic catalysis was recently established as a very new heterogeneous catalytic reaction platform.^[6,24,25,32,33,37,88–92] Recent experimental and theoretical reports present plasmonic catalysis as a route to concentrate and direct the energy of visible light to adsorbed molecules, enhance the rate of chemical reactions, and offer a pathway to control the reaction selectivity. SPs can decay and transfer energy identical to that of incident photons to hot-electrons with kinetic energies above Fermi level. Stronger laser intensity produces more surface plasmon quantum's, subsequently producing a large density of hot-electrons generated from the plasmon decay. The hot-electrons can jump into the unoccupied resonant molecular energy level on the surface of Ag/Au metal. As the hot electrons jump on the molecules, the molecular potential energy surface (PES) can be changed from a state of neutral to temporal negative-ion. Energy from hot electrons above the Fermi surface can transfer intramolecular vibrational energy during the interactions, in which case the energy barrier of the chemical reactions decreases. In some cases,^[29] hot electrons provide kinetic energy and result in a temporal negative-ion PES. But in some cases,^[37] additional electrons are also needed in the surface catalysis reaction. Therefore, hot electrons provide two or three important contributions to plasmonic catalysis.

A study in 2010 revealed convincing evidence of plasmon catalysis of PATP to DMAB by LSPs.^[24] As shown in **Figure 9**,

compare with the SERS and normal Raman spectra of PATP, it was found that additional Raman peaks are at 1143, 1390, and 1432 cm^{-1} . However, simulated SERS spectra of PATP on Ag₅ clusters could not be reproduced very well. Unexpectedly, the Raman spectrum of DMAB (Figure 9d) is well reproduced by SERS spectra of PATP in Ag sol.^[24] All the three strongly enhanced peaks of DMAB represent symmetric a_g vibrational modes, strongly indicating the formation of DMAB from PATP through the N = N bond. These peaks are assigned to the a_{g12} , a_{g16} , and a_{g17} symmetric vibrational modes, respectively.

Meanwhile, Tian's group also found the same conclusion with more confident evidence, which revealed by SERS spectra and desorption electro-spectra ionization mass spectrometry spectra.^[25] The plasmon assisted reactions of PATP to DMAB were experimentally well confirmed by surface mass spectrometry (SMS), and electrochemistry, and it was found that the results are well consistent with the calculations. The SMS spectra were obtained from the PATP-adsorbed silver electrode after illuminated using a high power laser.^[25] As shown in **Figure 10**, the peaks of SMS spectra at 245.5 and 164 m z^{-1} could be assigned to "H+S–Ph–N = N–Ph–S" fragment and "K+S–Ph–NH₂", respectively. The peak of 245.5 m z^{-1} in Figure 10a working as a control cannot be observed. It was found that the formation of DMAB was produced from PATP excited by a high power laser. Moreover, the SERS spectra also indicate that DMAB can be synthesized successfully, which is commercially unavailable

To provide further evidence for plasmon-driven chemical reaction of PATP being converted to DAMB, it is necessary to

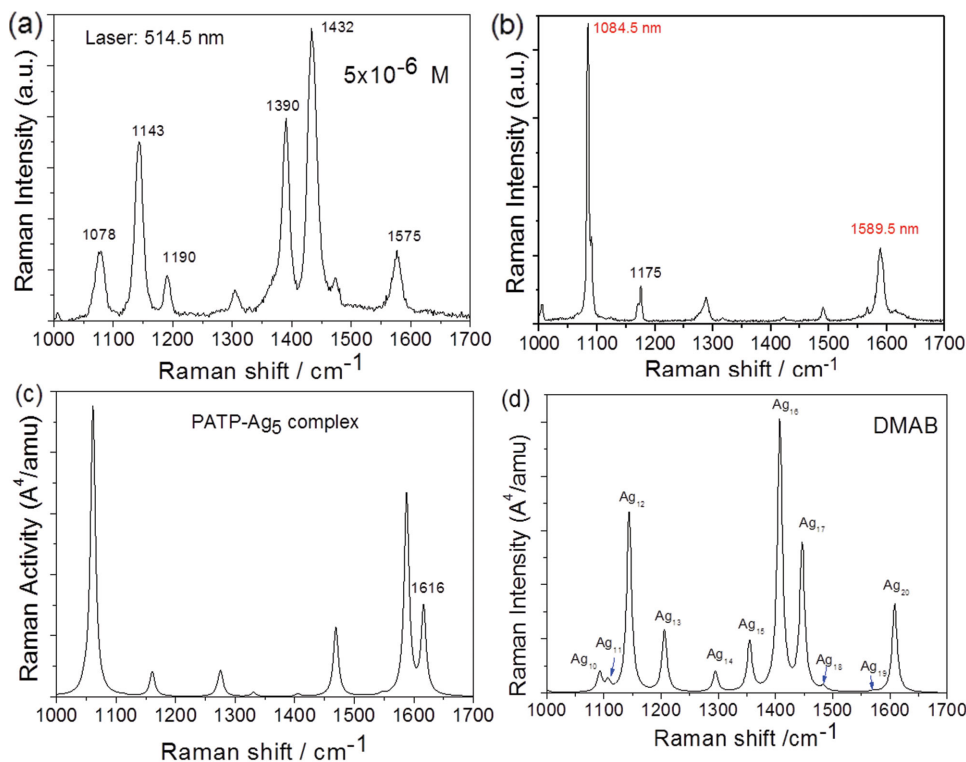


Figure 9. a) Experimental SERS spectra of DMAB excited at 514.5 nm, b) the experimental normal Raman spectrum of PATP, c) theoretical SERS spectrum of a PATP-Ag₅ complex, and d) simulated Raman spectrum of DMAB. Reproduced with permission.^[24] Copyright 2010, American Chemical Society.

ascertain the real SERS spectra of PATP. By using the system of nanoparticles, the strong surface plasmonic resonance make the chemical reaction easy, and the real SERS spectra of PATP would not be discovered, which is a challenge of observation of the real SERS spectra of PATP. As shown in **Figure 11**, by using the SERS substrate of silver nanowire on silver, film the SERS spectra of PATP was same as the normal Raman spectra of PATP, where the DMAB modes at 1140, 1390, 1432 cm⁻¹ were not obtained (see **Figure 12**), and the SERS spectra are the same

as the Raman spectrum of PATP powder.^[89] Furthermore, the laser intensity dependent dynamics of surface catalytic reaction that PATP react to DMAB were also monitored (see **Figure 13**). The reason that the genuine SERS spectrum was successfully observed is that the enhancement of electromagnetic field at the gap of silver nanowire and silver film is much weaker than that in the normal hot-spots of silver or gold nanoparticles.^[89]

Then similar experimental results have also reported by many other groups.^[90–93] The mechanism of Plasmon-driven

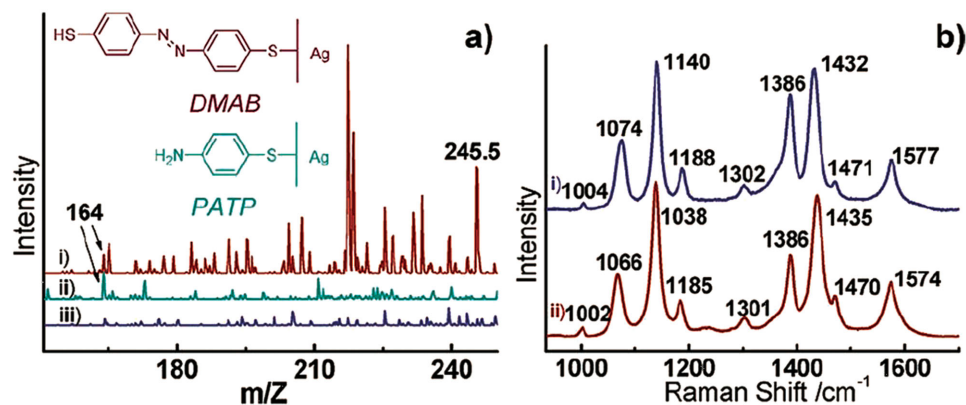


Figure 10. a) DESI (desorption electrospray ionization)-MS spectra of PATP adsorbed on roughened Ag electrodes, illuminated with laser light i), without any irradiation ii), and a roughened Ag-free spectrum of PATP iii). b) i) Raman spectrum of PATP, and ii) DMAB on the roughened Ag electrode excited by laser light at a power density of ca. 1×10^8 mW cm⁻². Reproduced with permission.^[25] Copyright 2010, American Chemical Society.

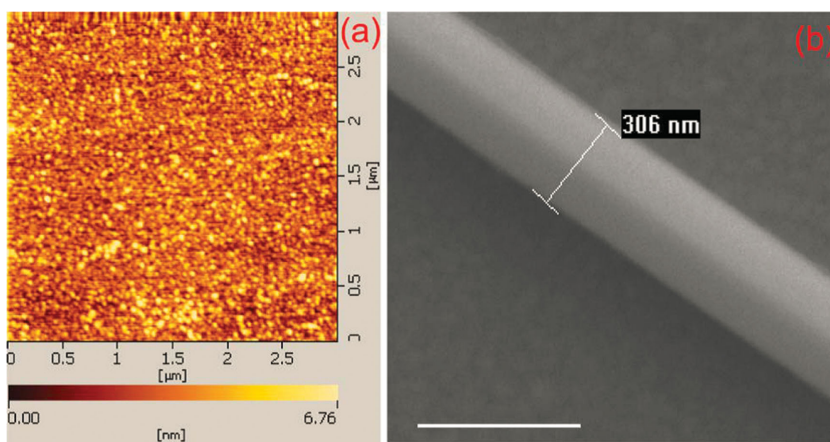


Figure 11. a) AFM image of Ag film, and b) a typical SEM image of Ag nanowire-Ag film system. The scale bar in b) is 500 nm. Reproduced with permission.^[89] Copyright 2012, Royal Society of Chemistry.

chemical reaction has been also reported by Xu et al.^[90] and Tian et al.,^[30] respectively.

4.2.2. Remote-Excitation Plasmon-Driven Chemical Reactions by Nanoparticle–Nanowire Systems

Remote SERS has been introduced into plasmonic catalysis in which propagating SPPs behaved as carriers for catalysis

and sensing.^[53–55] By using remote SERS technology, the plasmon catalyzed reaction of PATP to DMAB was demonstrated at the junction at the nanowire and nanoparticle system.^[53] As shown in **Figure 14**, the SEM image and optical photo of propagating SPPs (**Figure 14a,b**) reveal that the distance is about 3.4 μm and the size of the excitation spot is about 130 nm. Maximal signals can be obtained when the polarization of excited laser was parallel to the nanowire waveguide. The white spot at the gap of the nanowire and nanoparticle indicates that light converted by propagating SPPs from the another side of the silver nanowire. Remote plasmon driven chemical reaction of PATP to DMAB occur by using remote SERS, and the fluctuation of polarization intensity of incident light shown by the spectra could be explained by the polarization dependence of propagating SPPs as discussed above. However, the plasmonic catalysis of PATP to DMAB cannot occur at the excited side of the nanowire, which is local SERS (**Figure 14e**), because the electromagnetic field intensity at the excited side is weaker than that at the hot spot of the junction, as is essential to plasmonic catalysis. The corresponding optical image and image of the Raman mode of Ag_{17} of DMAB confirm that the plasmonic catalysis occurs only at the junction of the nanowire and nanoparticle by remote SERS.

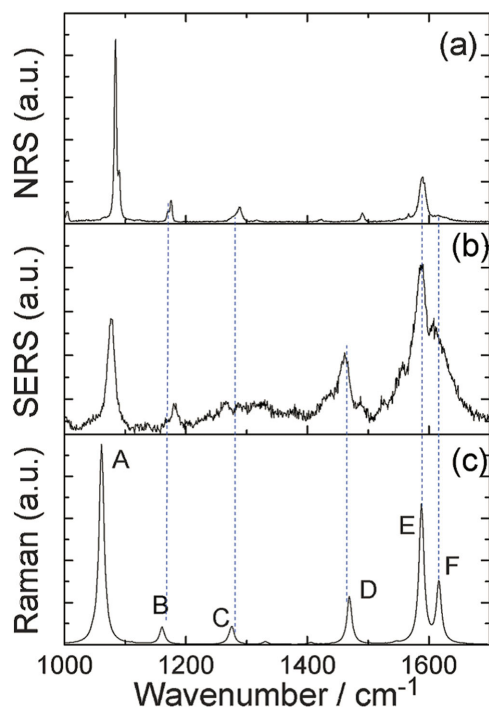


Figure 12. a) NRS spectrum of PATP powder, b) SERS spectrum of PATP, and c) the simulated Raman spectrum of PATP adsorbed on Ag_5 cluster. Reproduced with permission.^[89] Copyright 2012, Royal Society of Chemistry.

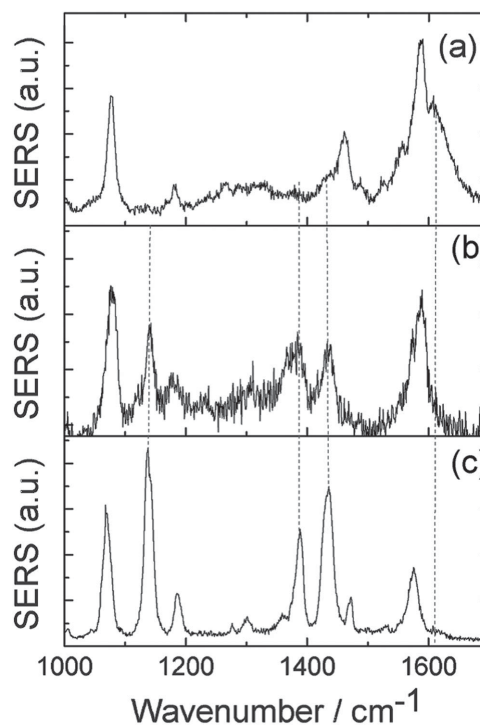


Figure 13. a,b) SERS spectra of PATP measured at the very beginning and after 60 s of laser radiating in Ag nanowire on Ag film system, respectively, and c) the SERS spectrum of DMAB in Ag aggregation system. Reproduced with permission.^[89] Copyright 2012, Royal Society of Chemistry.

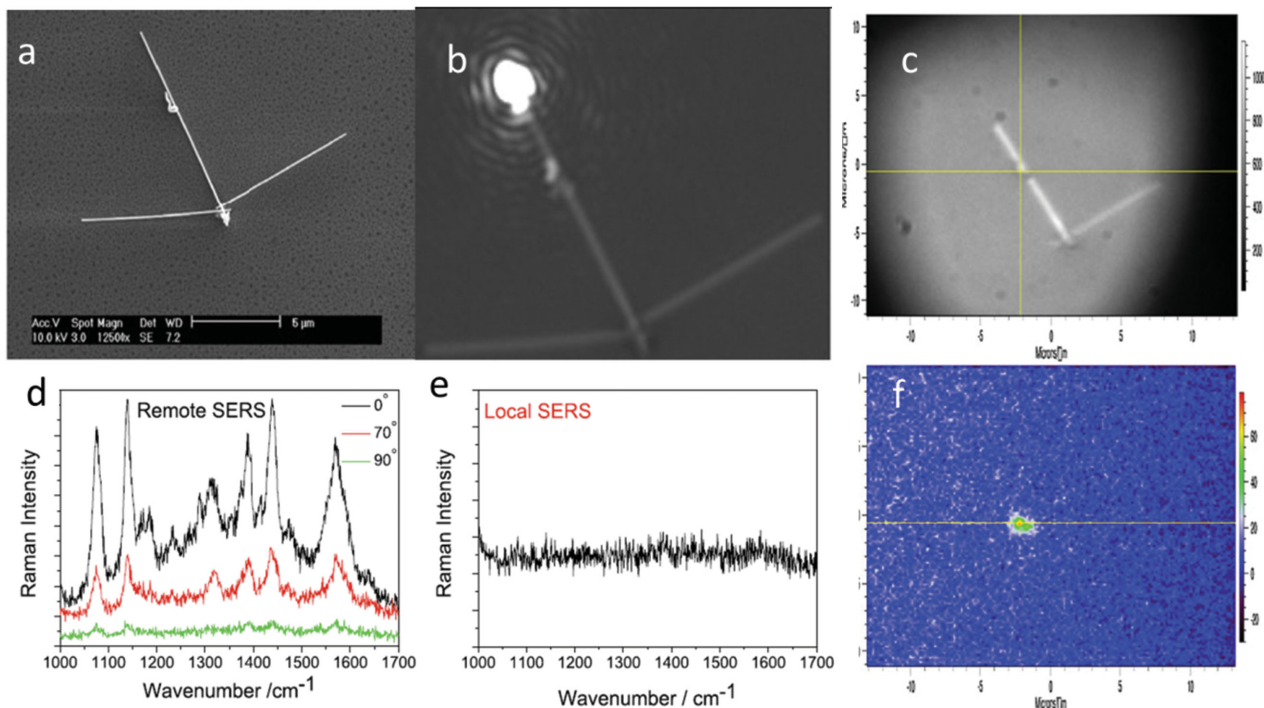


Figure 14. a) SEM image of Ag nanoparticles and nanowires system. b) Image of SPPs with the incident polarization along the nanowire. d) The incident polarization dependence of remote SERS spectra in this system. e) The local SERS spectrum collected at illuminating terminal. f) Raman image of Ag_{17} vibrational mode. Reproduced with permission.^[53] Copyright 2011, Springer.

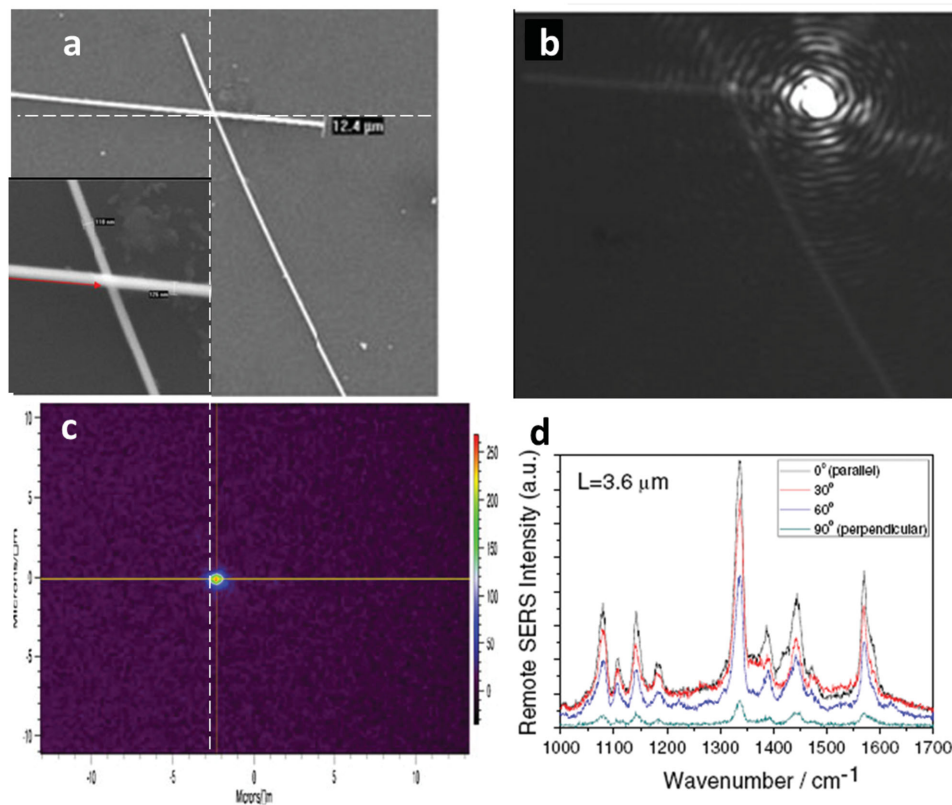


Figure 15. a) SEM image of silver crossed nanowires system. b) Corresponding image of SPPs of silver plasmonic waveguide. c) Corresponding Raman image of Ag_{17} vibrational mode. d) The polarization-dependent remote SERS spectra of DMAB. Reproduced with permission.^[54] Copyright 2013, Springer.

4.2.3. Remote Plasmon-Driven Chemical Reactions by Crossed-Nanowire System

In the remote SERS system of the single nanowire, the distance of remote excitation was decided by the length of nanowire. In contrast, in the nanoparticle–nanowire system, the hot spot at the nanogap of the nanoparticle and adjacent nanowire can be adjusted by changing the nanoparticle position along the nanowire. However, the distance between the nanogap and the excited side of nanowire is hard to control experimentally. A crossed nanowires system formed by two nanowires may overcome the aforementioned disadvantages. The junction of the crossed nanowires produces a hot spot that could be readily positioned through a 3D micromanipulator system under the optical microscope. We were thus able to investigate catalysis by remote SERS in crossed silver nanowires in recent report.^[54] The remote SERS spectra at the junction indicates that the reaction of 4NBT to DMAB could be induced by propagating SPPs under a laser excitation of 632.8 nm wavelength focused at the nanowire side (Figure 15). The optical image and corresponding SEM image of propagating SPPs are shown in Figure 15a,b. The magnified images show that the size of diameters of that two crossed nanowires were 126 and 110 nm, respectively. The clear white spot at the junction indicates that coupling photons emerged from propagating SPPs while the laser excited at one nanowire terminal was about 3.6 μm away. Distinct DMAB vibrational features (Figure 15d) are present in the remote SERS spectra obtained with various incident polarizations. These demonstrate that the surface catalysis reaction was remotely induced by propagating SPPs. The maximal intensity of remote SERS was observed while the polarization of incident laser was parallel to the nanowire. This result can be explained by the higher efficiency of SPPs propagation along the nanowire axis in the single-silver-nanowire system. To exclude the possibility that SERS signals obtained from the junction were due to background scattering or SPP propagation at the excited side, Raman images at the Ag_{17} vibrational mode of DMAB are shown in Figure 15c. The colored gap area indicates that remote plasmonic catalysis only occurred in the hot spot due to the strongly enhanced EM field. In addition, the time dependent properties of remote plasmon catalyzed reactions in such crossed nanowires system were also confirmed in this work.

4.2.4. Remote Plasmon-Driven Chemical Reactions by a Metal-Nanowire Array-Bundle System

In 2012, Moskovits' group reported another efficient remote SERS system by using nanowire bundle consists of nanowire array that produced by electrochemical deposition on a porous anodic alumina (PAA) template. Due to the strongly enhanced

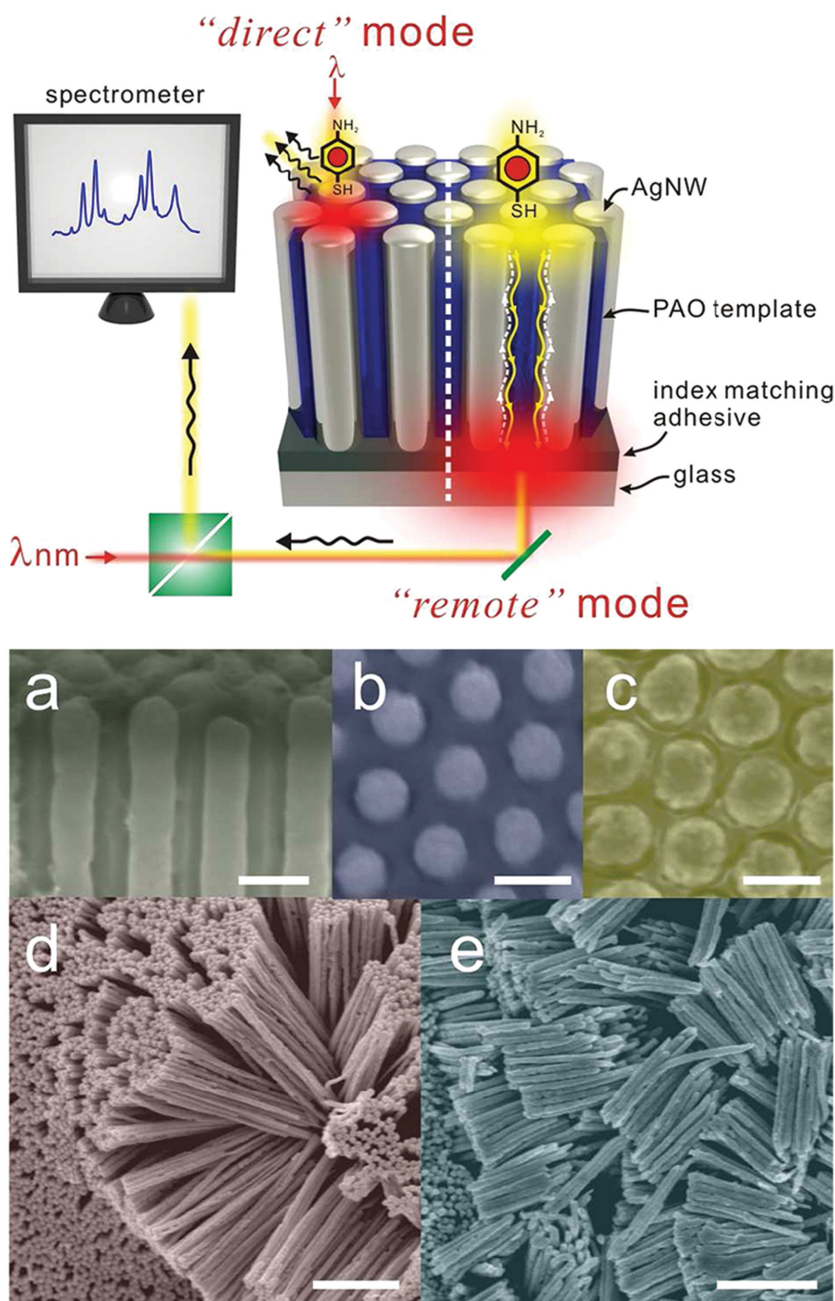


Figure 16. (top) The sketch of the remote and local SERS based on silver nanowire array bundles system. (bottom) SEM images of system. a) Lateral and b) top view SEM images of a silver nanowire array bundles system. c) Top view of system with 11 nm inter-wire gaps. d,e) systems with 2.2 μm length (33 nm gap) and 1 μm (11 nm gap) after dissolving the porous alumina oxide template. Reproduced with permission.^[55] Copyright 2012, American Chemical Society.

EM field at the nanowire gaps, this system were also used in plasmonic catalysis, such as water splitting and the reaction of PATP to DMAB.^[94–96] In this remote sensing system, the silver nanowire array was used as a probe, which can be attached to a catheter or an optical fiber to collect remote SERS signals in biological cell or liquids.^[55] The SEM images of probe structures and experiment setup are illustrated in **Figure 16**. The anodic alumina film at top was slightly dissolved to ensure that the PATP molecules can be attached to the Ag nanowire array. An index-matching adhesive was used to reduce the reflection from the interface between glass substrate and remote system. The bundles of silver nanowire with 11 and 33 nm gap dis-

tances are presented, while the distance between nanowires was about 100 nm. The lengths of the silver nanowire array were about 2.2 and $\approx 1 \mu\text{m}$ for 33 and 11 nm gap, respectively. As shown in the standard SERS, the incident laser was directed to focus on the top of the nanowires where the molecules were located. But for remote SERS, the incident laser was focused on the bottom glass substrate. In contrast to the above remote SERS systems, SPPs propagating along the silver nanowires originated not only from the incident laser, but also by the molecular Raman scattering in this nanowire array remote system. So the observation suggests that the remote distance was twice the length of nanowire array. Because of electrical resistance, SPPs propagating along the Ag nanowires could be attenuated exponentially as a function of the nanowire length, which was confirmed by the results on the remote SERS with different lengths ranging from 1 to 3 μm . The results also indicate that the Raman signals observed from larger nanowires (88 nm) were stronger than those from smaller nanowires (68 nm). The difference is due to the enhanced function of the narrower inter-nanowire gap as a hot spot and to the lower attenuation achieved with the larger nanowire.

As shown in **Figure 17**, excellent SERS and remote SERS spectra can be obtained by such a remote nanowire array system.^[55] Clearly, the plasmon catalyzed reaction of PATP to DMAB can be observed and monitored by remote probe, although here it was not comprehended that these SERS peaks were those of DMAB. The high remote SERS intensities indicate that the excited laser produced SPPs on the silver nanowire array can reach to the remote side of the nanowire; some energy was coupled out to create an optical near field in the gaps at the remote side where excited the molecules.

5. Conclusions and Perspectives

We have reviewed plasmonic waveguide for remote-excitation surface catalytic reactions in detail, including the synthesis methods of Ag nanowires, the property and physical mechanism of plasmonic waveguides, and the successful applications of plasmonic waveguides in the field of remote-excitation surface catalytic reactions. However, some challenges should be overcome in order to understand the full potential of remote plasmonic catalysis. More experimental and theoretical research, including on plasmon induced hot electrons, SPPs and plasmonic catalysis, is necessary in the near future so as to exploit the full potential of remote SERS systems. In addition, the distance of remote SERS based

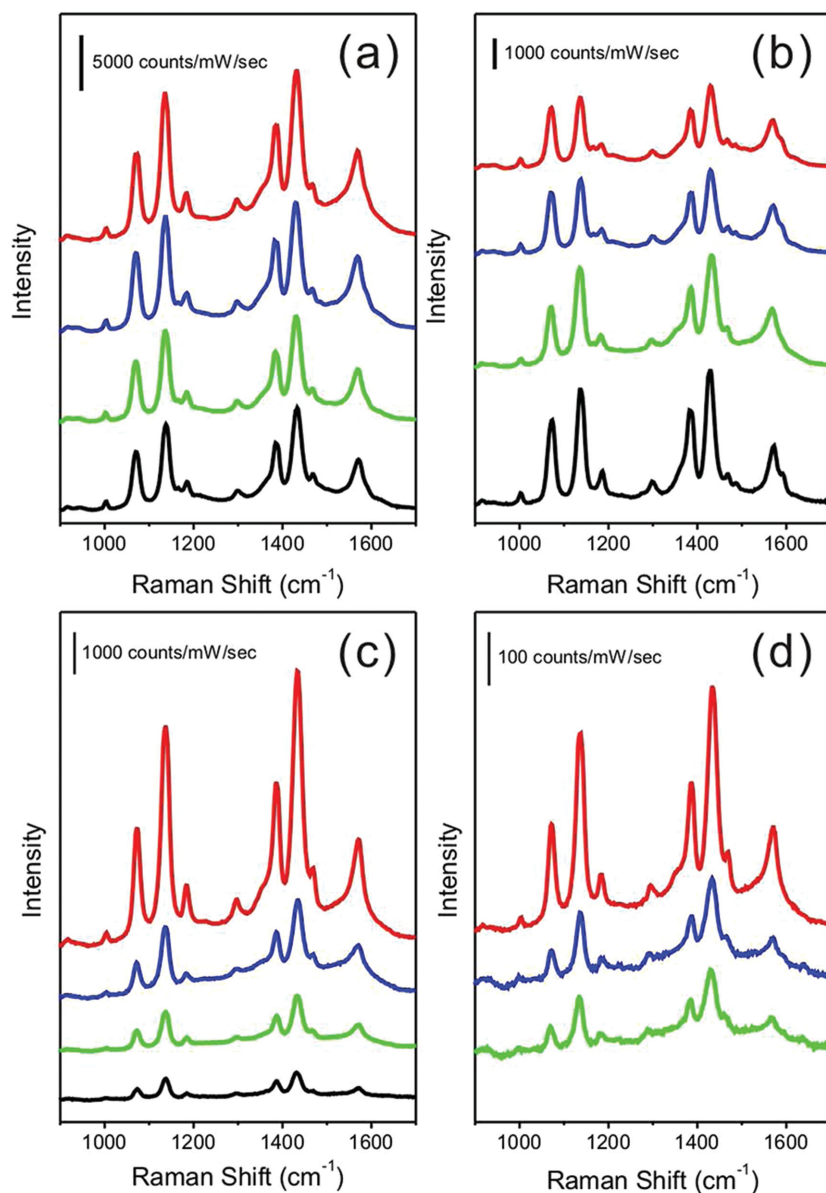


Figure 17. Averaged SERS spectra taken by a,b) direct excitation and c,d) remote excitation; a,c) gap of ≈ 11 nm with nanowire length of ≈ 920 nm (red), ≈ 1960 nm (blue), ≈ 2520 nm (green), and ≈ 3300 nm (black), respectively. b,d) Gap of ≈ 33 nm with NW length of ≈ 860 nm (red), ≈ 1880 nm (blue), ≈ 2160 nm (green), and ≈ 2880 nm (black), respectively. Reproduced with permission.^[55] Copyright 2012, American Chemical Society.

on metal nanowire waveguide is limited to a dozen μm . In the future, more methods for the synthesis of plasmonic materials should be developed, since the yield of Ag nanowire synthesized by chemical methods is limited. Stronger plasmonic waveguides should be created by nano-antenna, since the stronger intensity of plasmonic waveguide can result in a larger probability of chemical reaction. For example, with two or more Ag nanowires crossed, and two or more lasers simultaneously radiated on the terminals of the nanowires, collecting the remote SERS signals at the cross point. Better substrates should be developed for decreasing the loss of plasmonic waveguide on the preparation along nanowires.

Acknowledgements

Z. Zhang and Y. Fang contributed equally to this work. This work was supported by the National Science Foundation of China (Grant No. 11304135, 91436102, 11374353), and the Program of Liaoning Key Laboratory of Semiconductor Light Emitting and Photocatalytic Materials. Z. Zhang thanks the support from the Alexander von Humboldt foundation. Y. Fang would like to thank the Kunt and Alice Wallenberg Foundation.

Received: June 23, 2015

Revised: July 10, 2015

Published online: October 28, 2015

- [1] R. H. Ritchie, *Phys. Rev.* **1957**, 106, 874.
- [2] J. M. Brockman, B. P. Nelson, R. M. Corn, *Annu. Rev. Phys. Chem.* **2000**, 51, 41.
- [3] M. T. Sun, Z. Zhang, P. Wang, Q. Li, F. Ma, H. Xu, *Light: Sci. Appl.* **2013**, 2, e112.
- [4] R. M. Stockle, Y. D. Suh, V. Deckert, R. Zenobi, *Chem. Phys. Lett.* **2000**, 318, 131.
- [5] Y. R. Fang, Z. L. Zhang, L. Chen, M. T. Sun, *Phys. Chem. Chem. Phys.* **2015**, 17, 783.
- [6] M. T. Sun, H. X. Xu, *Small* **2012**, 8, 2777.
- [7] M. Moskovits, *Rev. Mod. Phys.* **1985**, 57, 783.
- [8] H. Metiu, P. Dos, *Annu. Rev. Phys. Chem.* **1984**, 35, 507.
- [9] K. Kneipp, H. Kneipp, I. Itzkan, R. R. Dasari, M. S. Feld, *Chem. Rev.* **1999**, 99, 2957.
- [10] M. T. Sun, S. S. Liu, M. D. Chen, H. X. Xu, *J. Raman Spectrosc.* **2009**, 40, 137.
- [11] J. R. Lombardi, R. L. Birke, *Acc. Chem. Res.* **2009**, 42, 734.
- [12] E. Bailo, V. Deckert, *Chem. Soc. Rev.* **2008**, 37, 921.
- [13] A. Otto, *J. Raman Spectrosc.* **2005**, 36, 497.
- [14] S. X. Sheng, Z. L. Zhang, Y. R. Fang, M. T. Sun, unpublished.
- [15] S. Mukherjee, F. Libisch, N. Large, O. Neumann, L. V. Brown, J. Cheng, J. B. Lassiter, E. A. Carter, P. Nordlander, N. J. Halas, *Nano Lett.* **2013**, 13, 240.
- [16] S. Mukherjee, L. A. Zhou, A. M. Goodman, N. Large, C. Ayala-Orozco, Y. Zhang, P. Nordlander, N. J. Halas, *J. Am. Chem. Soc.* **2014**, 136, 64–67.
- [17] J. Lee, S. Mubeen, X. L. Ji, G. D. Stucky, M. Moskovits, *Nano Lett.* **2012**, 12, 5014.
- [18] H. M. Chen, C. K. Chen, C. J. Chen, L. C. Cheng, P. C. Wu, B. H. Cheng, Y. Z. Ho, M. L. Tseng, Y. Y. Hsu, T. S. Chan, J. F. Lee, R. S. Liu, D. P. Tsai, *ACS Nano* **2012**, 6, 7362.
- [19] Y. Tsuboi, R. Shimizu, T. Shoji, N. Kitamura, *J. Am. Chem. Soc.* **2009**, 131, 12623.
- [20] K. Ueno, S. Juodkakis, T. Shibuya, Y. Yokota, V. Mizeikis, K. Sasaki, H. Misawa, *J. Am. Chem. Soc.* **2008**, 130, 6928.
- [21] C. Deeb, C. Ecoffet, R. Bachelot, J. Plain, A. Bouhelier, O. Soppera, *J. Am. Chem. Soc.* **2011**, 133, 10535.
- [22] C. Hubert, A. Romyantseva, G. Lerondel, J. Grand, S. Kostcheev, L. Billot, A. Vial, R. Bachelot, P. Royer, S. H. Chang, S. K. Gray, G. P. Wiederrecht, G. Schatz, *Nano Lett.* **2005**, 5, 615.
- [23] C. J. Chen, R. M. Osgood, *Phys. Rev. Lett.* **1983**, 50, 1705.
- [24] Y. R. Fang, Y. Li, H. X. Xu, M. T. Sun, *Langmuir* **2010**, 26, 7737.
- [25] Y. F. Huang, H. P. Zhu, G. K. Liu, D. Y. Wu, B. Ren, Z. Q. Tian, *J. Am. Chem. Soc.* **2010**, 132, 9244.
- [26] M. T. Sun, Z. L. Zhang, H. R. Zheng, H. Xu, *Sci. Rep.* **2012**, 2, 647.
- [27] Z. Zhang, L. Chen, M. Sun, P. Ruan, H. Zheng, H. Xu, *Nanoscale* **2013**, 5, 3249.
- [28] M. Sun, Z. Zhang, Z. H. Kim, H. Zheng, H. Xu, *Chem. Eur. J.* **2013**, 19, 14958.
- [29] P. Christopher, H. Xin, S. Linic, *Nature Chem.* **2011**, 3, 467.
- [30] Y. F. Huang, M. Zhang, L. B. Zhao, J. M. Feng, D. Y. Wu, B. Ren, Z. Q. Tian, *Angew. Chem. Int. Edit.* **2014**, 53, 2353.
- [31] S. Navalon, M. de Miguel, R. Martin, M. Alvaro, H. Garcia, *J. Am. Chem. Soc.* **2011**, 133, 2218.
- [32] M. Sun, Z. Zhang, L. Chen, Q. Li, S. Sheng, H. Xu, P. Song, *Adv. Mater. Interfaces* **2014**, 1, 1300125.
- [33] Z. Zhang, S. Sheng, H. Zheng, H. Xu, M. T. Sun, *Nanoscale* **2014**, 6, 4903.
- [34] C. G. Silva, R. Juárez, T. Marino, R. Molinari, H. García, *J. Am. Chem. Soc.* **2011**, 133, 595.
- [35] W. L. Barnes, A. Dereux, T. W. Ebbesen, *Nature* **2003**, 424, 824.
- [36] M. W. Knight, H. Sobhani, P. Nordlander, N. J. Halas, *Science* **2011**, 332, 702.
- [37] B. Dong, Y. R. Fang, X. W. Chen, H. X. Xu, M. T. Sun, *Langmuir* **2011**, 27, 10677.
- [38] I. Goykhman, B. Desiatov, J. Khurgin, J. Shappir, U. Levy, *Nano Lett.* **2011**, 11, 2219.
- [39] A. O. Govorov, H. Zhang, Y. K. Gunko, *J. Phys. Chem. C* **2013**, 117, 16616.
- [40] L. Cui, P. Wang, X. Chen, Y. Fang, Z. Zhang, M. T. Sun, *Sci. Rep.* **2014**, 4, 7221.
- [41] Z. L. Zhang, T. Deckert-Gaudig, P. Singh, V. Deckert, *Chem Commun.* **2015**, 51, 3069.
- [42] Y. F. Huang, D. Y. Wu, H. P. Zhu, L. B. Zhao, G. K. Liu, B. Ren, Z. Q. Tian, *Phys. Chem. Chem. Phys.* **2012**, 14, 8484.
- [43] S. Linic, P. Christopher, H. Xin, A. Marimuthu, *Acc. Chem. Res.* **2013**, 46, 1890.
- [44] K. Ueno, H. Misawa, *J. Photochem. Photobiol. C: Photochem. Reviews* **2013**, 15, 31.
- [45] X. J. Chen, G. Cabello, D. Y. Wu, Z. Q. Tian, *J. Photochem. Photobiol. C: Photochem. Reviews* **2014**, 21, 54.
- [46] M. J. Kale, T. Avanesian, P. Christophe, *ACS Catal.* **2014**, 4, 116.
- [47] Z. Zhang, T. Deckert, V. Deckert, *Analyst* **2015**, 140, 4325.
- [48] J. A. Hutchison, S. P. Centeno, H. Odaka, H. Fukumura, J. Hofkensand, H. Uji-i, *Nano Lett.* **2009**, 9, 995.
- [49] Y. R. Fang, H. Wei, F. Hao, P. Nordlander, H. X. Xu, *Nano Lett.* **2009**, 9, 2049.
- [50] R. X. Yan, J. H. Park, Y. Choi, C. J. Heo, S. M. Yang, L. P. Lee, P. Yang, *Nanotechnol.* **2012**, 7, 191.
- [51] G. Lu, H. D. Keersmaecker, L. Su, B. Kenens, S. Rocha, E. Fron, C. Chen, P. Van Dorpe, H. Mizuno, J. Hofkens, J. A. Hutchison, H. Uji-i, *Adv. Mater.* **2014**, 26, 5124.
- [52] Y. Huang, Y. R. Fang, Z. L. Zhang, L. Zhu, M. T. Sun, *Light: Sci. Appl.* **2014**, 3, e199.
- [53] M. T. Sun, Y. X. Hou, Z. P. Li, L. W. Liu, H. X. Xu, *Plasmonics* **2011**, 6, 681.
- [54] P. Song, Y. Z. Li, Y. Q. Li, M. Y. Zhao, L. W. Liu, M. T. Sun, *Plasmonics* **2013**, 8, 249.
- [55] S. J. Lee, M. Moskovits, *J. Am. Chem. Soc.* **2012**, 134, 11384.
- [56] C. L. Chen, H. Furusho, H. Mori, *Nanotechnology* **2009**, 20, 405605.

- [57] P. Mohanty, I. Yoon, T. Kang, K. Seo, K. S. K. Varadwaj, W. Choi, Q. H. Park, J. P. Ahn, Y. D. Suh, H. Ihee, B. Kim, *J. Am. Chem. Soc.* **2007**, *129*, 9576.
- [58] H. Ditzlacher, A. Hohenau, D. Wagner, U. Kreibitz, M. Rogers, F. Hofer, F. R. Aussenegg, J. R. Krenn, *Phys. Rev. Lett.* **2005**, *95*, 257403.
- [59] J. Q. Hu, Q. Chen, Z. X. Xie, G. B. Han, R. H. Wang, B. Ren, Y. Zhang, Z. L. Yang, Z. Q. Tian, *Adv. Funct. Mater.* **2004**, *14*, 183.
- [60] X. X. Li, L. Wang, G. Q. Yan, *Cryst. Res. Technol.* **2011**, *46*, 427.
- [61] P. M. Ajayan, S. Iijima, *Nature* **1993**, *361*, 333.
- [62] Y. J. Han, J. M. Kim, G. D. Stucky, *Chem. Mater.* **2000**, *12*, 2068.
- [63] C. R. Martin, *Science* **1994**, *266*, 1961.
- [64] T. D. Lazzara, G. R. Bourret, R. B. Lennox, T. G. M. van de Ven, *Chem. Mater.* **2009**, *21*, 2020.
- [65] Z. A. Hu, T. Xu, R. J. Liu, H. L. Li, *Mater. Sci. Eng., A* **2004**, *371*, 236.
- [66] E. Braun, Y. Eichen, U. Sivan, G. Ben-Yoseph, *Nature* **1998**, *391*, 775.
- [67] N. R. Jana, L. Gearheart, C. J. Murphy, *Chem. Commun.* **2001**, 617.
- [68] S. H. Park, H. S. Shin, Y. H. Kim, H. M. Park, J. Y. Song, *Nanoscale* **2013**, *5*, 1864.
- [69] Y. G. Sun, Y. N. Xia, *Adv. Mater.* **2002**, *14*, 833.
- [70] Y. G. Sun, B. Gates, B. Mayers, Y. N. Xia, *Nano Lett.* **2002**, *2*, 165.
- [71] Y. G. Sun, Y. N. Xia, *Science* **2002**, *298*, 2176.
- [72] K. E. Korte, S. E. Skrabalak, Y. N. Xia, *J. Mater. Chem.* **2008**, *18*, 437.
- [73] B. Wiley, Y. G. Sun, Y. N. Xia, *Langmuir* **2005**, *21*, 8077.
- [74] J. T. Jiu, T. Tokuno, M. Nogi, K. Suganuma, *J. Nanopart. Res.* **2012**, *14*, 975.
- [75] J. Jiu, T. Araki, J. Wang, M. Nogi, T. Sugahara, S. Nagao, H. Koga, K. Suganuma, E. Nakazawa, M. Hara, H. Uchida, K. Shinozaki, *J. Mater. Chem. A* **2014**, *2*, 6326.
- [76] S. Coskun, B. Aksoy, H. E. Unalan, *Cryst. Growth Des.* **2011**, *11*, 4963.
- [77] X. L. Tang, M. Tsuji, P. Jiang, M. Nishio, S. M. Jang, S. H. Yoon, *Colloid. Surface. A* **2009**, *338*, 33.
- [78] M. Tsuji, M. Hashimoto, Y. Nishizawa, M. Kubokawa, T. Tsuji, *Chem. Eur. J.* **2005**, *11*, 440.
- [79] C. Chen, L. Wang, G. H. Jiang, Q. Yang, J. J. Wang, H. J. Yu, T. Chen, C. L. Wang, *Nanotechnology* **2006**, *17*, 466.
- [80] J. T. Jiu, T. Sugahara, M. Nogi, K. Suganuma, *J. Nanopart. Res.* **2013**, *15*, 1.
- [81] C. L. Tang, W. Sun, J. M. Lu, W. Yan, *J. Colloid. Interface Sci.* **2014**, *416*, 86.
- [82] S. H. Liu, B. M. Sun, J. G. Li, J. L. Chen, *Crystengcomm* **2014**, *16*, 244.
- [83] D. E. Chang, A. S. Sorensen, P. R. Hemmer, M. D. Lukin, *Phys. Rev. B* **2007**, *76*, 035420.
- [84] S. P. Zhang, H. Wei, K. Bao, U. Hakanson, N. J. Halas, P. Nordlander, H. X. Xu, *Phys. Rev. Lett.* **2011**, *107*, 096801.
- [85] R. M. Dickson, L. A. Lyon, *J. Phys. Chem. B* **2000**, *104*, 6095.
- [86] Y. R. Fang, M. T. Sun, *Light: Sci. Appl.* **2015**, *4*, e294.
- [87] Y. Z. Huang, Y. R. Fang, M. T. Sun, *J. Phys. Chem. C* **2011**, *115*, 3558.
- [88] H. Zhu, X. Ke, X. Yang, S. Sarina, H. Liu, *Angew. Chem. Int. Ed.* **2010**, *49*, 9657.
- [89] X. Tian, L. Chen, H. Xu, M. T. Sun, *RSC Adv.* **2012**, *2*, 8289.
- [90] P. Xu, L. Kang, N. H. Mack, K. S. Schanze, X. Han, H. L. Wang, *Sci. Rep.* **2013**, *3*, 2997.
- [91] S. Zong, Z. Wang, J. Yang, Y. Cui, *Anal. Chem.* **2011**, *83*, 4178.
- [92] J. Ye, J. A. Hutchison, H. Uji-i, J. Hofkens, L. Lagae, G. Maes, G. Borghs, P. Van Dorpe, *Nanoscale* **2012**, *4*, 1606.
- [93] V. Canpean, M. Iosin, S. Astilean, *Chem. Phys. Lett.* **2010**, *500*, 277.
- [94] S. Mubeen, J. Lee, N. Singh, S. Kramer, G. D. Stucky, M. Moskovits, *Nature Nanotechnol.* **2013**, *8*, 247.
- [95] J. Lee, S. Mubeen, X. Ji, G. D. Stucky, M. Moskovits, *Nano Lett.* **2012**, *12*, 5014.
- [96] S. Mubeen, G. Hernandez-Sosa, D. Moses, J. Lee, M. Moskovits, *Nano Lett.* **2011**, *11*, 5548.